Reactivity of [Fe_4S_4] Clusters toward C1 Substrates: Mechanism, Implications and Potential Applications

CHI CHUNG LEE, MARTIN T. STIEBRITZ AND YILIN HU*

Department of Molecular Biology and Biochemistry, University of California, Irvine, California 92697-3900, United States

RECEIVED ON DATE GOES HERE.

CONSPECTUS

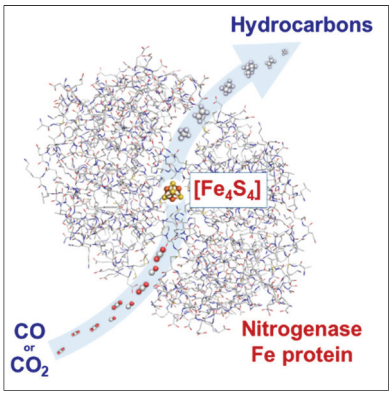

FeS proteins are metalloproteins prevalent in the metabolic pathways of most organisms, playing key roles in a wide range of essential cellular processes. A member of this protein family, the Fe protein of nitrogenase is a homodimer that contains a redox-active [Fe_4S_4] cluster at the subunit interface and an ATP-binding site within each subunit. During catalysis, the Fe protein serves as the obligate electron donor for its catalytic partner, transferring electrons concomitant with ATP hydrolysis to the cofactor site of the catalytic component to enable substrate reduction. The effectiveness of Fe protein in electron transfer is reflected by the unique reactivity of nitrogenase toward small-molecule substrates. Most notably, nitrogenase is capable of catalyzing the ambient reduction of N_2 and CO into NH_4^+ and hydrocarbons, respectively, in reactions that parallel the important industrial Haber-Bosch and Fischer-Tropsch processes. Other than participating in nitrogenase catalysis, the Fe protein also functions as an essential factor in nitrogenase assembly, which again highlights its capacity as an effective, ATP-dependent electron donor.

Recently, the Fe protein of a soil bacterium, *Azotobacter vinelandii*, was shown to act as a reductase on its own and catalyze the ambient conversion of CO_2 to CO at its [Fe_4S_4] cluster either under *in vitro* conditions when a strong reductant is supplied, or under *in vivo* conditions through the action of an unknown electron donor(s) in the cell. Subsequently, the Fe protein of a mesophilic methanogenic organism, *Methanosarcina acetivorans*, was shown to catalyze the *in vitro* reduction of CO_2 and CO into hydrocarbons under ambient conditions, illustrating an impact of protein scaffold on the redox properties of the [Fe_4S_4] cluster and the reactivity of the cluster toward C1 substrates. This reactivity was further traced to the [Fe_4S_4] cluster itself, as a synthetic [Fe_4S_4] compound was shown to catalyze the reduction of CO_2 and CO to hydrocarbons in solutions in the presence of a strong reductant. Together, these observations pointed to an inherent ability of the [Fe_4S_4] clusters and, possibly, the FeS clusters in general, to catalyze C1-substrate reduction. Theoretical calculations have led to the proposal of a plausible reaction pathway that involves the formation of hydrocarbons via aldehyde-like intermediates, providing an important framework for further mechanistic investigations of FeS-based activation and reduction of C1 substrates.

In this account, we summarize the recent work leading to the discovery of C1-substrate reduction by protein-bound and free [Fe_4S_4] clusters, as well as the current mechanistic understanding of this FeS-based reactivity. In addition, we briefly discuss the evolutionary implications of this discovery and potential applications that could be developed to enable FeS-based strategies for the ambient recycling of unwanted C1 wastes into useful chemical commodities.

Iron sulfur (FeS) proteins are key players in biological processes, serving a variety of functions that range from electron transfer and enzyme catalysis to DNA synthesis and gene regulation.[1-5] Collectively termed the Fe protein, the reductase component of nitrogenase is a member of the FeS protein family that employs a nucleotide-dependent energy transduction mechanism for electron transfer during catalysis.[6-9] Encoded by the *nifH* gene, the Fe protein of the well-studied Mo-nitrogenase from a soil bacterium, *Azotobacter vinelandii* (designated *Av*NifH), is a homodimer that contains a subunit-bridging [Fe_4S_4] cluster and one MgATP-binding site within each subunit. During catalysis, *Av*NifH is believed to undergo conformational changes upon binding and hydrolysis of MgATP, which permits a decrease in the reduction potential of its [Fe_4S_4] cluster concomitant with a productive binding of this protein to its catalytic partner, MoFe protein (designated *Av*NifDK).[1,10,11] Together, these events facilitate efficient inter-protein transfer of electrons from the [Fe_4S_4] cluster of *Av*NifH, via a so-called P-cluster ([Fe_8S_7]),[10] to the M-cluster (or cofactor; [*R*-homocitrate-$MoFe_7S_9C$])[12] of *Av*NifDK, where substrate reduction takes place (Figure 1A; Figure S1).

The capacity of Fe protein in electron transfer is reflected by the unique reactivity of nitrogenase toward small-molecule substrates, such as N_2, CO and C_2H_2.[1,13-15] Of all reactions catalyzed by nitrogenase, the reductions of N_2 and CO, respectively, to ammonia and hydrocarbons are particularly important because of their energy- and environment-related significance. The two reactions mirror the industrial Haber-Bosch[16,17] and Fischer-Tropsch[18] processes, which are used for ammonia and carbon fuel production. However, contrary to their industrial parallels, the reductions of N_2 and CO by nitrogenase occur under ambient conditions, and they use H^+/e^- instead of H_2 as the reducing source, highlighting the power of this enzyme—owing largely to the efficacy of its unique reductase component—in small-molecule activation from the

perspective of chemical energy. Other than serving as the obligate electron donor for nitrogenase catalysis, the Fe protein also plays an essential role in the biosynthesis of nitrogenase. Interacting with apo *Av*NifDK at the α/β interface, *Av*NifH reductively couples a pair of [Fe_4S_4]-like clusters into a P-cluster concomitant with ATP hydrolysis (Figure 1B).[19-22] Likewise, *Av*NifH interacts with the biosynthetic scaffold protein *Av*NifEN (a homolog to *Av*NifDK in sequence and structure), reducing and inserting Mo along with homocitrate into a [Fe_8S_9] precursor and maturing this precursor into a fully assembled M-cluster in an ATP-dependent manner (Figure 1C).[19,20,23-25]

The physiological functions of the Fe protein in nitrogenase catalysis and assembly underscore the effectiveness of this protein as an electron donor to its redox partner; whereas at the same time, questions have arisen as to whether the Fe protein can act as a reductase on its own, as its unique [Fe_4S_4] center is nearly surface-exposed and could undergo facile redox changes between various oxidation states (0, +1, +2) to enable substrate binding and reduction.[1,26-28] Consistent with this suggestion, our recent studies have shown that the Fe proteins can reduce C1 substrates (*i.e.*, CO_2, CO) into various products (*i.e.*, CO, hydrocarbons) under ambient conditions (Figure 1D),[29,39] when electrons are supplied *in vitro* by an artificial reductant or by an unknown electron donor(s) *in vivo*. Furthermore, our studies have demonstrated that this reactivity is inherent to the FeS centers in these proteins, as [Fe_4S_4] clusters that exist freely in solutions can catalyze the same ambient reactions as the Fe protein-associated [Fe_4S_4] clusters in the presence of a strong reductant.[30] Our theoretical calculations have led to the proposal of a plausible reaction pathway that involves the formation of hydrocarbons via aldehyde-like intermediates, which provides an important framework for further mechanistic investigations of FeS-based activation and reduction of C1 substrates.

This account summarizes the recently-discovered artificial reactivity of protein-associated and free [Fe_4S_4] clusters toward C1 substrates, as well as the current mechanistic understanding of this reactivity. In addition, some thoughts are provided on the plausible evolutionary implications of this discovery and how it could be explored for developing FeS-based strategies for ambient conversion of unwanted C1 wastes into useful products in the future.

Reduction of C1 substrates by protein-bound and free [Fe_4S_4] clusters

The ability of a protein-bound [Fe_4S_4] cluster to reduce CO_2 was first described for *Av*NifH under *in vivo* and *in vitro* conditions.[29] In an *in vitro* assay, both the nucleotide-free and ATP-bound forms of *Av*NifH can reduce CO_2 to CO in minor yields in the presence of an artificial reductant, dithionite ($E^{0'}$= −0.436 V at pH 7),[29] where its [Fe_4S_4] cluster assumes the +1 oxidation state (Figure 2A, *left*). The yield of CO production by ATP-bound *Av*NifH is 30% higher than its nucleotide-free counterpart, which is consistent with a decrease in the reduction potential of its [Fe_4S_4] cluster by ~100 mV in the presence of ATP.[29] Substitution of dithionite for a stronger reductant, europium(II) diethylenetriaminepentaacetic acid (Eu^{II}–DTPA; $E^{0'}$= −1.14 V at pH 8),[30,31] results in a notable increase of product yield, which can be accounted for by the presence of the [Fe_4S_4] cluster of *Av*NifH in the "super-reduced", all-ferrous or 0 oxidation state. The yield of CO increases with increasing Eu^{II}-DTPA concentrations, reaching a total turnover number (TON) of ~8 under optimized reaction conditions (Figure 2A, *middle*)[30] Unlike the reaction driven by dithionite, the reaction driven by Eu^{II}-DTPA is nucleotide-independent as far as the product yield is concerned (Figure 2A, *middle*), which is likely due to a lack of impact of ATP-binding on the reduction potential of the all-ferrous [Fe_4S_4] cluster. The correlation between the [Fe_4S_4] center and the CO_2-reducing activity of *Av*NifH has been

established through EPR analysis, which reveals a decrease/disappearance of the $[Fe_4S_4]^{+}$-specific S=1/2 signal (perpendicular-mode) of the dithionite-reduced *Av*NifH (Figure 2B)[29] or the $[Fe_4S_4]^{0}$-specific g=16.4 signal (parallel-mode) of the Eu^{II}–DTPA-reduced *Av*NifH (Figure 2C)[29] that corresponds to an oxidation of the cluster concomitant with a transfer of electrons from the reduced cluster to the substrate CO_2. It should be noted that the spectra of both dithionite- and Eu^{II}–DTPA-reduced *Av*NifH proteins display a small, perpendicular-mode signal at $g\approx2$ in the presence of CO_2 (Figure 2B, D),[29] which suggests an impact of interaction with, or binding of, CO_2 or CO_2-derived intermediates on the electronic properties of the $[Fe_4S_4]$ cluster.

The ambient conversion of CO_2 to CO can also be accomplished *in vivo* by a *nifDK*-deletion strain of *A. vinelandii*, which expresses *Av*NifH as the sole component of Mo-nitrogenase under N_2-fixing (*i.e.*, ammonia-depleted) growth conditions (Figure 2A, *right*).[29] Upon exhaustion of ammonia in the growth medium, the expression of *Av*NifH is upregulated concomitant with a significant increase of the activity of the strain to reduce CO_2 to CO, showing a TON of 110 at 40% CO_2 (Figure 2A, *right*). The much higher *in vivo* activity of *Av*NifH in CO_2 reduction could originate from a reducing intracellular environment of *A. vinelandii* rendered by its effective O_2-protection mechanisms[32] and/or the presence of a physiological electron donor(s) for *Av*NifH[33,34] that poises its $[Fe_4S_4]$ cluster in the all-ferrous, 0 oxidation state to enable efficient CO_2 reduction. The latter scenario is particularly intriguing, as it may bear relevance to the long-standing question in the nitrogenase field of whether the Fe protein-associated cluster could directly shuttle between the all-ferrous, $[Fe_4S_4]^{0}$ state and the oxidized, $[Fe_4S_4]^{2+}$ state (instead of between the commonly acknowledged $[Fe_4S_4]^{1+}$ and $[Fe_4S_4]^{2+}$ states) for a two-electron transfer event that could improve the energy economy of nitrogenase catalysis under physiological conditions.[35,36]

Interestingly, even the all-ferrous, $[Fe_4S_4]^0$-state *Av*NifH (*e.g.*, generated by Eu^{II}-DTPA) cannot reduce CO into additional products (Figure 3A),[30] which could explain why CO is detected as the only product of CO_2 reduction by *Av*NifH.[29,30] Moreover, the oxidized, $[Fe_4S_4]^{2+}$-state *Av*NifH [generated by the oxidant indigodisulfonate (IDS)] can catalyze the oxidation of CO to CO_2 considerably faster than the reduction of CO_2 to CO (Figure 3B)[29]—a feature resembling that of the CO/CO_2-interconverting enzyme, carbon monoxide dehydrogenase (CODH)[37-39]—which could contribute further to the low CO yield of *Av*NifH.[29] In comparison, the Fe protein from a methanogenic organism, *Methanosarcina acetivorans* (designated *Ma*NifH),[30,40] which shares 72% sequence homology with its *A. vinelandii* counterpart, is capable of reducing CO_2 past CO into hydrocarbons (Figure 3C);[30] yet, it cannot catalyze the reverse reaction that oxidizes CO to CO_2 (Figure 3B).[30] Like *Av*NifH, *Ma*NifH can reduce CO_2 to CO in the presence of Eu^{II}-DTPA; yet, it displays a different pattern of product formation than *Av*NifH, showing a decrease in the yield of CO concomitant with an increase in the yields of C1 (CH_4), C2 (C_2H_4, C_2H_6) and C3 (C_3H_6, C_3H_8) hydrocarbon products upon an increase of the Eu^{II}-DTPA concentration beyond 20 mM (Figure 3C).[30] The total TON (~5) of the *Ma*NifH-catalyzed reaction, on the other hand, remains roughly unchanged despite a shift from CO-formation toward hydrocarbon-formation at increasing Eu^{II}-DTPA concentrations (Figure 3C), pointing to a dependence of product distribution on the available amount of electrons in the reaction.[30] Other than reducing CO_2, *Ma*NifH can also reduce CO directly to hydrocarbons (Figure 3A),[30] achieving a much higher TON (~30) than that accomplished in the reduction of CO_2 (Figure 3C).[30] Notably, the CO- and CO_2-reductions by *Ma*NifH show similar product distributions (Figure 3D),[30] suggesting routing of the reduction of CO_2 via CO or CO-derived intermediates.

The observed discrepancy in the reactivities of *Av*NifH and *Ma*NifH toward C1 substrates is somewhat surprising, particularly given the high degree of sequence homology between the two proteins. One factor that could contribute to this discrepancy is a difference in the reduction potentials of these proteins, with the broader reactivity of *Ma*NifH toward CO_2 and CO accounted for by an experimentally-observed lower reduction potential of its cluster ($[Fe_4S_4]^{1+/2+}$: $E^0 = -395$ mV) than that of its counterpart in *Av*NifH ($[Fe_4S_4]^{1+/2+}$: $E^0 = -301$ mV).[30] In addition, a difference in the binding affinities of these proteins to the intermediate CO may also explain their differential reactivities toward C1 substrates. The fact that the product yield of *Ma*NifH saturates quickly with increasing concentrations of CO[30] lends support to this argument, suggesting a high CO-affinity of *Ma*NifH that potentially biases this protein toward CO reduction and C–C bond formation instead of releasing CO as an end product of CO_2 reduction.

The nearly surface-exposed location of the $[Fe_4S_4]$ cluster in the Fe protein[11,27,28] points to the distinct possibility that $[Fe_4S_4]$ clusters existing freely in solutions may have the same C1-substrate-reducing activities as their protein-bound counterparts. Indeed, in the presence of 20 mM Eu^{II}–DTPA, a synthetic $[PPh_4]_2[Fe_4S_4(SCH_2CH_2OH)_4]$ compound (Figure 4A; designated $[Fe_4S_4]^{Syn}$) can reduce CO_2 and CO at TONs of 0.3 and 0.4 (Figure 4B),[30] respectively, to C1 and C2 hydrocarbons (CH_4, C_2H_4, C_2H_6) in an aqueous buffer (Figure 4C).[30] When the same reactions are conducted in an organic solvent (dimethylformamide (DMF)) and driven by 20 mM samarium(II) iodide (SmI_2; $E^{0\prime} = -1.5$ V in DMF)[41] along with a proton source (triethylammonium tetrafluoroborate $[Et_3NH(BF_4)]$), the yields of hydrocarbons increase significantly, reaching TONs of 15.8 and 89.7 (Figure 4D),[30] respectively, in the reactions of CO_2- and CO-reduction by $[Fe_4S_4]^{Syn}$; moreover, the increase in product yield is accompanied by an expansion of the product profile (CH_4, C_2H_4, C_2H_6, C_3H_6, C_3H_8, C_4H_8, C_4H_{10}) and extension

of hydrocarbon chain lengths (up to C4) (Figure 4E).[30] The negligible amounts of hydrocarbon formation in control reactions containing $FeCl_3$ solutions with equimolar Fe—either in the presence or absence of Na_2S— provide strong, if indirect, proof that the CO_2/CO-reducing activities do not result from the small, Fe/S-breakdown products of the $[Fe_4S_4]^{Syn}$ clusters (Figure 4D).[30] Further, the fact that the maximum TONs of the free $[Fe_4S_4]^{Syn}$ cluster are notably higher than those of the *Ma*NifH-associated $[Fe_4S_4]$ cluster in C1-substrate reduction could be attributed to an increased accessibility of the reaction sites in solutions of free clusters. Together, these observations firmly establish the ability to reduce C1 substrates as an inherent catalytic feature of the $[Fe_4S_4]$ clusters.

Mechanistic insights into the reduction of C1 substrates by $[Fe_4S_4]$ clusters

In light of the newly-discovered activity of $[Fe_4S_4]$ clusters in C1-substrate reduction, density functional theory (DFT) calculations were first performed on *Av*NifH to provide mechanistic insights into the binding and activation of CO_2 by a protein-bound $[Fe_4S_4]$ cluster. Based on these calculations, activation of CO_2 by *Av*NifH is achieved through binding of C to a Fe atom of the all-ferrous $[Fe_4S_4]^0$ cluster in the singlet spin state (S = 0), as well as hydrogen-bonding interactions between O and the side chains of a pair of highly conserved Arg100 residues (designated $Arg100^A$ and $Arg100^B$)—one from each subunit of *Av*NifH (Figure 5A).[29] Such a binding pattern renders the CO_2 moiety in an activated, carboxylate-like conformation concomitant with charge redistribution to the O atoms, which facilitates polarization and, eventually, scission of the C–O bond to yield the product, CO. Based on the calculated binding energy (*ca.* −5 kcal/mol),[29] coordination of CO_2 by the protein-bound cluster is rather weak, which could account for the low activity of *Av*NifH in CO_2 reduction. Moreover, coordination of

C to Fe makes it unlikely for the protein to generate formate via hydrogenation of the C atom of CO_2, which is consistent with the absence of formate from the product profile of *Av*NifH-catalyzed CO_2 reduction.[29]

The reaction pathway following the binding and activation of CO_2 was then examined by DFT calculations of CO_2 reduction by synthetic $[Fe_4S_4]$ clusters.[30] One plausible mechanism involves protonation of the coordinated CO_2 moiety, followed by proton-coupled electron transfer, which initiates cleavage of a water molecule and renders the cluster in a CO-bound, $[Fe_4S_4]^+$ state (Figure 5B, *step 3*). The reaction pathway becomes branched at this point: one branch involves energetically-disfavored dissociation of CO (Figure 5B, *step 4*), which could contribute to the overall low activity of CO_2 reduction; whereas the other branch involves proton-coupled electron transfer to the Fe-bound CO moiety, which results in an aldehyde-like, Fe-formyl species that undergoes exothermic proton-coupled electron transfer steps, concomitant with dissociation of a water molecule, to generate a Fe-methyl species that eventually yields CH_4 (Figure 5B, *steps 6-12*). Coordination of a second CO for C–C bond formation could then occur at several mechanistic branching points, where a primary C1 species remains bound to the cluster. One likely scenario involves exothermic binding of CO to the methyl-bound Fe site, which yields a Fe-acetyl intermediate via migratory insertion (Figure 5B, *steps 14 and 15*). Subsequent reduction and proton-transfer steps lead to dissociation of a water molecule and formation of an Fe-ethyl species that eventually gives rise to C_2H_6 (Figure 5B, *steps 16-20*). Energetically, it is plausible for the cluster to continue to use the same mechanism for chain extension beyond C2, which begins with coordination of CO to an ethyl-bound Fe site and formation of a Fe-propionyl species via migratory insertion.

While alternative pathways can be proposed for the same reaction, the mechanism presented above aligns well with our experimental observations.[30] For example, consistent with the observed increase in hydrocarbon/CO ratio with increasing concentrations of the reductant (Figure 3C),[30] the calculations suggest that a constant high supply of electrons shifts the reaction from CO-dissociation (Figure 5B, *step 4*) toward CO-reduction (Figure 5B, *step 6*). Moreover, in corroboration with the experimental observation of a higher yield of CH_4 than C2 products under conditions of high electron fluxes (Figure 4E),[30] the calculations point to a competition between C–C coupling and protonation of the Fe-methyl species and a bias toward formation of CH_4 via the latter route.[30] Likewise, the experimentally observed bias toward short-chain product formation (Figure 4C, E)[30] could be explained by the calculations, which suggest that the probability of chain elongation >C2 is significantly lower than that of the release of C2 products.[30] Perhaps more excitingly, the calculation-predicted appearance of aldehyde-like intermediates is supported by experimental data showing the ability of the synthetic [Fe_4S_4] clusters to reduce formaldehyde (CH_2O) to CH_4 at a TON of ~16 (Figure 5C),[30] highlighting the possibility to test and refine the calculation-based model(s) in order to gain a better mechanistic understanding of the FeS-based CO_2/CO reduction.

Evolutionary implications and potential applications of FeS-based C1-reducing activities

It is interesting to consider the ability of [Fe_4S_4] clusters to convert CO_2 and CO and hydrocarbons in an evolutionary context, as this reactivity may have implications for the prebiotic evolution of organic molecules. Previous studies have pointed to a role of Fe- or FeS-containing minerals around undersea hypothermal vents in generating hydrocarbons and other organic molecules in the presence of CO_2.[42-45] Moreover, CO has been shown to react with

CH_3SH on coprecipitated FeS and NiS to form carboxylic acids, carbohydrates and amino acids via a presumed CH_3-CO-SCH_3 intermediate, leading to the proposal of a prebiotic carbon fixation pathway employed by the earliest organisms for the emergence of primordial lipids, sugars and peptides/proteins on Earth.[46-49] In light of these findings, the reduction of CO_2 and CO by spontaneously-generated FeS clusters in a speculated, highly-reducing early atmosphere could represent another prebiotic route of carbon fixation; only in this case, CO_2 and CO were converted to small alkenes and alkanes that could be used as carbon and/or electron sources by certain methane- and ethene-assimilating microbes.[50,51] Given the postulation that the methane- and CO-rich atmosphere and the anoxic oceans in the Archean era were inhabited by iron- and sulfur-metabolizing microbes,[48] it is plausible that these microbes might evolve the prebiotic route of carbon fixation via FeS clusters into a reaction catalyzed by FeS enzymes, which enabled the production of small hydrocarbons via secondary metabolism of these microbes and the subsequent use of these products by hydrocarbon-assimilating organisms in the same microbial community. The CO_2- and CO-reducing activities of the nitrogenase Fe proteins, therefore, may represent an evolutionary relic of the functions of these FeS enzymes, and the disparate reactivities of *Ma*NifH and *Av*NifH toward CO_2 may reflect different adaptabilities of the methanogenic and non-methanogenic organisms to their surroundings, particularly when the CO_2-rich habitat of methanogens is taken into consideration.

Regardless of its relevance to evolution, the ability of protein-bound and solution-state [Fe_4S_4] clusters to reduce CO_2 and CO to hydrocarbons points to the possibility of developing FeS-based catalysts for the ambient conversion of unwanted C1 wastes into useful chemical commodities. One major hurdle for this quest, however, is the low efficiency of the [Fe_4S_4] clusters in C1-substrate reduction. Thus, considerations must be given to both the FeS center and the protein

scaffold when developing strategies to improve the reactivity of FeS catalysts toward C1 substrates. With regard to the FeS center, it is interesting to note a striking analogy between the DFT-predicted structure of the CO_2-activated *Av*NifH and a carboxylate–nickel intermediate proposed previously for the CO_2-bound Ni–CODH (Figure 6).[29,52] Such a similarity is not particularly surprising given the resemblance of the C-cluster ([$NiFe_4S_4$])—the active site of Ni-CODH—to a [Fe_4S_4] cluster. However, the presence of a pair of Ni (a Lewis base) and Fe (a Lewis acid) atoms in the C-cluster could, at least in part, account for a significantly higher activity of Ni–CODH than the Fe protein in CO_2 activation. As such, strategies could be developed to generate heterometallic FeS clusters—a feat that has been accomplished both chemically and biochemically[53-55]—in hopes of improving the CO_2-reducing activity of this reaction. With regard to the protein scaffold, a comparison between the crystal structure of *Av*NifH and the homology model of *Ma*NifH in the all-ferrous state reveals a higher accessibility of the [Fe_4S_4] cluster (Figure 7)[27,40] and, consequently, a possible change of the reduction potential of the cluster in *Ma*NifH, both of which could contribute to an improved CO_2-reducing activity of this protein. This observation is in line with our preliminary crystallographic analysis of *Ma*NifH, as well as our previous determination of the reduction potential of the $[Fe_4S_4]^{1+/2+}$ couple in *Ma*NifH, which is *ca.* 90 mV lower than that of the $[Fe_4S_4]^{1+/2+}$ couple in *Av*NifH. It is conceivable, therefore, that the protein scaffold can be modified to modulate the reactivity of the FeS center toward CO_2/CO while providing an added advantage of stabilizing the FeS center to achieve further improvement of this reactivity.

Once a "re-designed" FeS catalyst is generated upon optimization of the FeS center and/or the protein scaffold, there are two approaches that can be explored to develop FeS-based applications of ambient CO_2/CO conversion. One approach involves attachment of the FeS

catalyst, either in the isolated form or in the protein-bound state, to an electrode, which would permit a constant supply of electrons to the reaction at a desired potential. A recent study has revealed a "re-ignition" of the *Av*NifH-catalyzed reaction of CO_2 reduction upon repeated addition of Eu^{II}-DTPA,[29] which provides strong support for the possibility to develop a continuous, electrode-driven reaction system to sustain this reactivity and maximize the product yield. Moreover, previous studies have demonstrated a variation of product profiles at different reduction potentials and/or electron fluxes,[29,30] which further points to the utility of an electrode-based method in tuning product profiles toward desired products. In this context, it is important to note the development of highly efficient, electrode-based metal catalysts, such as iron-tetraphenylporphyrin complexes, which reduce CO_2 to CO with Faradaic efficiencies of >90% and turnover numbers of ~50 million in 4 h.[56,57] Conceivably, some of the general principles to achieve high efficiencies of these molecular Fe catalysts could be adapted for future development of electrode-based FeS catalysts with improved efficiencies to convert CO_2 to hydrocarbons. The second approach involves introduction of the re-designed, protein-bound FeS catalysts into appropriate microbial hosts to enable the *in vivo* CO_2 conversion by these catalysts. A recent study[58] has demonstrated the ability of V-nitrogenase—a natural variant of Mo-nitrogenase—to perform *in vivo* reduction of CO to hydrocarbons (C_2H_4, C_2H_6, C_3H_8) at a TON of 750 in a culture grown under N_2-fixing conditions, as well as a further increase of TON by more than 10-fold upon intermittent 'relaxation' of the culture in air. While a direct reduction of CO_2 by nitrogenase is not observed under *in vivo* conditions, a two-step process could be developed by coupling the *in vivo* reduction of CO_2 to CO by Fe protein with the *in vivo* reduction of CO to hydrocarbons by the complete nitrogenase enzyme. Such a whole-cell approach would represent an interesting "reverse" evolution of the unique reactivity of FeS

catalysts toward C1 substrates and facilitate future development of a feedstock-free approach to cost-efficient biofuel production.

AUTHOR INFORMATION

Corresponding Author

*E-mail: yilinh@uci.edu.

Author Contributions

The manuscript was written through contributions of all authors. All authors have given approval to the final version of the manuscript.

Funding

This work was supported by NSF Career grant CHE-1651398 (to Y.H.).

Notes

The authors declare no competing financial interest.

Biographical Information

Chi Chung Lee received a B.S. degree from the University of California, San Diego and a Ph.D. from the University of California, Irvine, where he is currently an Assistant Project Scientist.

Martin T. Stiebritz received B.S., M.S. and Ph.D. degrees from the University of Erlangen-Nuremberg, Germany. He was a postdoctoral fellow and a senior researcher at ETH Zurich and is now an Assistant Specialist at the University of California, Irvine.

Yilin Hu received a B.S. degree from FuDan University, China, and a Ph.D. from Loma Linda University. She was a postdoctoral fellow and is now an Assistant Professor of Molecular Biology and Biochemistry at University of California, Irvine.

ABBREVIATIONS

NifDK, nitrogenase MoFe protein; NifH, nitrogenase Fe protein

REFERENCES

(1) Burgess, B.K.; Lowe, D.J. Mechanism of molybdenum nitrogenase. *Chem. Rev.* **1996**, *96,* 2983–3012.

(2) Schilter, D.; Camara, J.M.; Huynh, M.T.; Hammes-Schiffer, S.; Rauchfuss, T.B. Hydrogenase enzymes and their synthetic models: The role of metal hydrides. *Chem. Rev.* **2016**, *116,* 8693–8749.

(3) Mühlenhoff, U.; Hoffmann, B.; Richter, N.; Rietzschel, N.; Spantgar, F.; Stehling, O.; Uzarska, M.A.; Lill, R. Compartmentalization of iron between mitochondria and the cytosol and its regulation. *Eur. J. Cell Biol.* **2015**, *94,* 292–308.

(4) O'Brien, E.; Holt, M.E.; Thompson, M.K.; Salay, L.E.; Ehlinger, A.C.; Chazin, W.J.; Barton, J.K. The [4Fe4S] cluster of human DNA primase functions as a redox switch using DNA charge transport. *Science* **2017**, *355,* 813.

(5) Mettert, E.L.; Kiley, P.J. Fe-S proteins that regulate gene expression. *Biochim. Biophys. Acta.* **2015**, *1853,* 1284–1293.

(6) Koonin, E.V. A superfamily of ATPases with diverse functions containing either classical or deviant ATP-binding motif. *J. Mol. Biol.* **1993**, *229,* 1165-1174.

(7) Pai, E.F.; Krengel, U.; Petsko, G.A.; Goody, R.S.; Kabsch, W.; Wittinghofer, A. Refined crystal structure of the triphosphate conformation of H-ras p21 at 1.35 A resolution: implications for the mechanism of GTP hydrolysis. *EMBO J.* **1990**, *9,* 2351-2359.

(8) Story, R.M.; Steitz, T.A. Structure of the recA protein-ADP complex. *Nature* **1992**, *355,* 374-376.

(9) Howard, J.B.; Rees, D.C. Nitrogenase: a nucleotide-dependent molecular switch. *Annu. Rev. Biochem.* **1994**, *63,* 235-264.

(10) Schindelin, H.; Kisker, C.; Schlessman, J.L.; Howard, J.B.; Rees, D.C. Structure of ADP x AlF_4^--stabilized nitrogenase complex and its implications for signal transduction. *Nature* **1997**, *387,* 370-376.

(11) Rees, D.C.; Akif Tezcan, F.; Haynes, C.A.; Walton, M.Y.; Andrade, S.; Einsle, O.; Howard, J.B. Structural basis of biological nitrogen fixation. *Philos. Trans. A Math. Phys. Eng. Sci.* **2005**, *363,* 971-984.

(12) Spatzal, T.; Aksoyoglu, M.; Zhang, L.; Andrade, S.L.; Schleicher, E.; Weber, S.; Rees, D.C.; Einsle, O. Evidence for interstitial carbon in nitrogenase FeMo cofactor. *Science* **2011**, *334*, 940.

(12) Hoffman, B.M.; Lukoyanov, D.; Yang, Z.Y.; Dean, D.R.; Seefeldt, L.C. Mechanism of nitrogen fixation by nitrogenase: the next stage. *Chem Rev.* **2014**, *114,* 4041-4062.

(14) Lee, C.C.; Hu, Y.; Ribbe, M.W. Vanadium nitrogenase reduces CO. *Science* **2010**, *329,* 642.

(15) Hu. Y.; Lee, C.C.; Ribbe, M.W. Extending the carbon chain: hydrocarbon formation catalyzed by vanadium/molybdenum nitrogenases. *Science* **2011**, *333,* 753-755.

(16) Schlögl, R. Catalytic synthesis of ammonia-a "never-ending story"? *Angew. Chem. Int.*

Ed. Engl. **2003**, *42,* 2004-2008.
(17) Cherkasov, N.; Ibhadon, A.O.; Fitzpatrick, P. A review of the existing and alternative methods for greener nitrogen fixation. *Chem. Eng. Process.* **2015**, *90,* 24-33.
(18) Rofer-DePoorter, C.K. A comprehensive mechanism for the Fischer-Tropsch synthesis. *Chem. Rev.* **1981**, *81,* 447-474.
(19) Hu, Y.; Ribbe, M.W. Biosynthesis of the metalloclusters of nitrogenases. *Annu. Rev. Biochem.* **2016**, *85,* 455-483.
(20) Ribbe, M.W.; Hu, Y.; Hodgson, K.O.; Hedman, B. Biosynthesis of nitrogenase metalloclusters. *Chem. Rev.* **2014**, *114,* 4063-4080.
(21) Corbett, M.C.; Hu, Y.; Fay, A.W.; Tsuruta, H.; Ribbe, M.W.; Hodgson, K.O.; Hedman, B. Conformational differences between *Azotobacter vinelandii* nitrogenase MoFe proteins as studied by small-angle X-ray scattering. *Biochemistry* **2007**, *46,* 8066-8074.
(22) Hu, Y.; Fay, A.W.; Lee, C.C.; Ribbe, M.W. P-cluster maturation on nitrogenase MoFe protein. *Proc. Natl. Acad. Sci. USA* **2007**, *104,* 10424-10429.
(23) Kaiser, J.T.; Hu, Y.; Wiig, J.A.; Rees, D.C.; Ribbe, M.W. Structure of precursor-bound NifEN: a nitrogenase FeMo cofactor maturase/insertase. *Science* **2011**, *331,* 91-94.
(24) Fay, A.W.; Blank, M.A.; Lee, C.C.; Hu, Y.; Hodgson, K.O.; Hedman, B.; Ribbe, M.W. Spectroscopic characterization of the isolated iron-molybdenum cofactor (FeMoco) precursor from the protein NifEN. *Angew. Chem. Int. Ed. Engl.* **2011**, *50,* 7787-7790.
(25) Hu, Y.; Corbett, M.C.; Fay, A.W.; Webber, J.A.; Hodgson, K.O.; Hedman, B.; Ribbe, M.W. Nitrogenase Fe protein: A molybdate/homocitrate insertase. *Proc. Natl. Acad. Sci. USA* **2006**, *103,* 17125-17130.
(26) Angove, H.C.; Yoo, S.J.; Münck, E.; Burgess, B.K. An all-ferrous state of the Fe protein of nitrogenase. Interaction with nucleotides and electron transfer to the MoFe protein. *J. Biol. Chem.* **1998**, *273,* 26330-26337.
(27) Strop, P.; Takahara, P.M.; Chiu, H.; Angove, H.C.; Burgess, B.K.; Rees, D.C. Crystal structure of the all-ferrous $[4Fe\text{-}4S]^0$ form of the nitrogenase iron protein from *Azotobacter vinelandii. Biochemistry* **2001**, *40,* 651-656.
(28) Georgiadis, M.M.; Komiya, H.; Chakrabarti, P.; Woo, D.; Kornuc, J.J.; Rees, D.C. Crystallographic structure of the nitrogenase iron protein from *Azotobacter vinelandii. Science* **1992**, *257,* 1653-1659.
(29) Rebelein, J.G.; Stiebritz, M.T.; Lee, C.C.; Hu, Y. Activation and reduction of carbon dioxide by nitrogenase iron proteins. *Nat. Chem. Biol.* **2017**, *13,* 147-149.
(30) Stiebritz, M.T.; Hiller, C.J.; Sickerman, N.S.; Lee, C.C.; Tanifuji, K.; Ohki, Y.; Hu, Y. Ambient conversion of CO_2 to hydrocarbons by biogenic and synthetic $[Fe_4S_4]$ clusters. Nat. Catal. 2018, 1, 444-451.
(31) Vincent, K.A.; Tilley, G.J.; Quammie, N.C.; Streeter, I.; Burgess, B.K.; Cheesman, M.R.; Armstrong, F.A. Instantaneous, stoichiometric generation of powerfully reducing states of protein active sites using Eu(II) and polyaminocarboxylate ligands. *Chem. Commun. (Camb).* **2003**, *20,* 2590-2591.
(32) Orme-Johnson, W.H.; Sands, R.H. *Iron-Sulfur Proteins*, Lovenberg, W: Academic Press, New York & London, 1973; pp. 195-238
(33) Lowery, T.J.; Wilson, P.E.; Zhang, B.; Bunker, J.; Harrison, R.G.; Nyborg, A.C.; Thiriot, D.; Watt, G.D. Flavodoxin hydroquinone reduces *Azotobacter vinelandii* Fe protein to the all-ferrous redox state with a S = 0 spin state. *Proc. Natl. Acad. Sci. USA* **200**6, *103,* 17131-17136.

(34) Jacobs, D.; Watt, G.D. Nucleotide-assisted [Fe_4S_4] redox state interconversions of the *Azotobacter vinelandii* Fe protein and their relevance to nitrogenase catalysis. *Biochemistry* **2013**, *52,* 4791-4799.
(35) Howard, J.B.; Rees D.C. How many metals does it take to fix N_2? A mechanistic overview of biological nitrogen fixation. *Proc. Natl. Acad. Sci. USA* **2006**, *103,* 17088-17093.
(36) Erickson, J.A.; Nyborg, A.C.; Johnson, J.L.; Truscott, S.M.; Gunn, A.; Nordmeyer, F.R.; Watt, G.D. Enhanced efficiency of ATP hydrolysis during nitrogenase catalysis utilizing reductants that form the all-ferrous redox state of the Fe protein. *Biochemistry* **1999**, *38,* 14279-14285.
(37) Jeoung, J.H.; Fesseler, J.; Goetzl, S.; Dobbek, H. Carbon monoxide. Toxic gas and fuel for anaerobes and aerobes: carbon monoxide dehydrogenases. *Met. Ions. Life Sci.* **2014**, *14,* 37-69.
(38) Kung, Y.; Drennan, C.L. A role for nickel-iron cofactors in biological carbon monoxide and carbon dioxide utilization. *Curr. Opin. Chem. Biol.* **2011**, *15,* 276-283.
(39) Can, M.; Armstrong, F.A.; Ragsdale, S.W. Structure, function, and mechanism of the nickel metalloenzymes, CO dehydrogenase, and acetyl-CoA synthase. *Chem. Rev.* **2014**, *114,* 4149-4174.
(40) Hiller, C.J.; Stiebritz, M.T.; Lee, C.C.; Liedtke, J.; Hu, Y. Tuning electron flux through nitrogenase with methanogen iron protein homologues. *Chemistry* **2017**, *23,* 16152-16156.
(41) Sickerman, N.S.; Hu, Y.; Ribbe, M.W. Activation of CO_2 by vanadium nitrogenase. *Chem. Asian. J.* **2017**, *12,* 1985-1996.
(42) Proskurowski, G.; Lilley, M.D.; Seewald, J.S.; Früh-Green, G.L.; Olson, E.J.; Lupton, J.E.; Sylva, S.P.; Kelley, D.S. Abiogenic hydrocarbon production at lost city hydrothermal field. *Science* **2008**, *319*, 604-607.
(43) McDermott, J.M.; Seewald, J.S.; German, C.R.; Sylva, S.P. Pathways for abiotic organic synthesis at submarine hydrothermal fields. *Proc. Natl. Acad. Sci. USA* **2015**, *112,* 7668-7672.
(44) Novikov,Y.; Copley, S.D. Reactivity landscape of pyruvate under simulated hydrothermal vent conditions. *Proc. Natl. Acad. Sci. USA* **2013**, *110,* 13283-13288.
(45) Roldan, A.; Hollingsworth, N.; Roffey, A.; Islam, H.U.; Goodall, J.B.; Catlow, C.R.; Darr, J.A.; Bras, W.; Sankar, G.; Holt, K.B.; Hogarth, G.; de Leeuw, N.H. Bio-inspired CO_2 conversion by iron sulfide catalysts under sustainable conditions. *Chem. Commun. (Camb)*. **2015**, *51,* 7501-7504.
(46) Huber, C.; Wächtershäuser, G. Activated acetic acid by carbon fixation on (Fe,Ni)S under primordial conditions. *Science* **1997**, *276,* 245-247.
(47) Scheidler, C.; Sobotta, J.; Eisenreich, W.; Wächtershäuser, G.; Huber, C. Unsaturated C3,5,7,9-monocarboxylic acids by aqueous, one-pot carbon fixation: possible relevance for the origin of life. *Sci. Rep.* **2016**, *6,* 27595.
(48) Huber, C.; Wächtershäuser, G. Alpha-Hydroxy and alpha-amino acids under possible Hadean, volcanic origin-of-life conditions. *Science* **2006**, *314,* 630-632.
(49) Huber, C.; Wächtershäuser, G. Peptides by activation of amino acids with CO on (Ni,Fe)S surfaces: implications for the origin of life. *Science* **1998**, *281,* 670-672.
(50) Roslev, P.; Iversen, N.; Henriksen, K. Oxidation and assimilation of atmospheric methane by soil methane oxidizers. *Appl. Environ Microbiol.* **1997**, *63,* 874-880.

(51) Coleman, N.V.; Spain, J.C. Distribution of the coenzyme M pathway of epoxide metabolism among ethene- and vinyl chloride-degrading Mycobacterium strains. *Appl. Environ. Microbiol.* **2003**, *69,* 6041-6046.
(52) Jeoung, J.H.; Dobbek, H. Carbon dioxide activation at the Ni,Fe-cluster of anaerobic carbon monoxide dehydrogenase. *Science* **2007**, *318,* 1461-1464.
(53) Moura, I.; Moura, J.J.G.; Munck, E.; Papaefthymiou, V.; LeGall, J. Evidence for the formation of a cobalt-iron-sulfur ($CoFe_3S_4$) cluster in *Desulfovibrio gigas* ferredoxin II. *J. Am. Chem. Soc.* **1986**, *108,* 349-351.
(54) Surerus, K.K.; Munck, E.; Moura, I.; Moura, J.J.G.; LeGall, J. Evidence for the formation of a $ZnFe_3S_4$ cluster in *Desulfovibrio gigas* ferredoxin II. *J. Am. Chem. Soc.* **1987**, *109,* 3805–3807.
(55) Kovacs, J.A.; Holm, R.H. Assembly of vanadium-iron-sulfur cubane clusters from mononuclear and linear trinuclear reactants *J. Am. Chem. Soc.* **1986**, *108,* 340-341.
(56) Costentin, C.; Drouet, S.; Robert, M.; Savéant, J.M. A local proton source enhances CO_2 electroreduction to CO by a molecular Fe catalyst. *Science* **2012**, *338*, 90–94.
(57) Costentin, C.; Passard, G.; Robert, M.; Savéant, J.M. Ultraefficient homogeneous catalyst for the CO_2-to-CO electrochemical conversion. *Proc. Natl. Acad. Sci. U. S. A.* **2014**, *111*, 14990–14994.
(58) Rebelein, J. G.; Lee, C. C.; Hu, Y.; Ribbe, M. W. The *in vivo* hydrocarbon formation by vanadium nitrogenase follows a secondary metabolic pathway. *Nat. Commun.* **2016**, *7*, 13641.

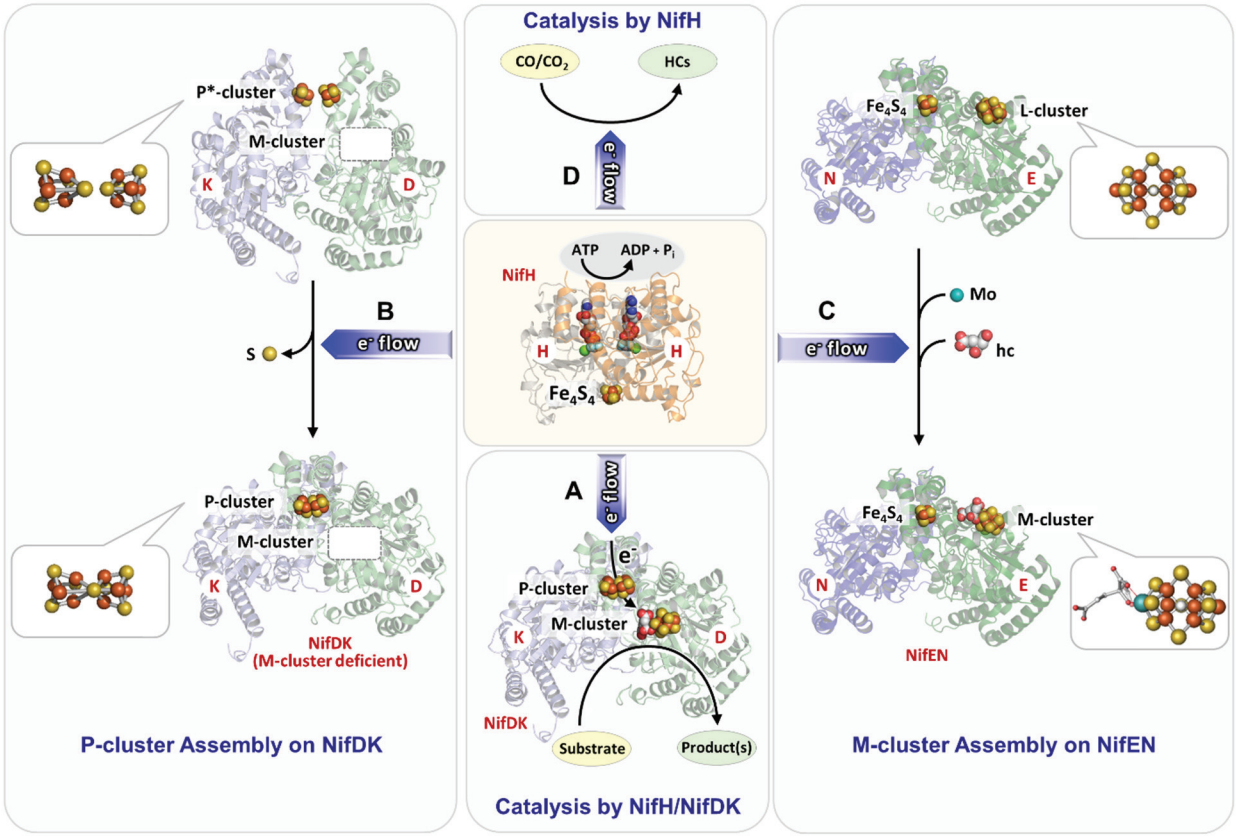

Figure 1. Functions of Fe protein as an electron donor for nitrogenase catalysis and assembly or as an independent reductase of C1 substrates. All functions of the Fe protein (NifH) are carried out by its [Fe_4S_4] cluster, which is capable of (A) transferring electrons via the P-cluster ([Fe_8S_7]) to the M-cluster (or cofactor; [*R*-homocitrate-$MoFe_7S_9C$]) of its catalytic partner, MoFe protein (NifDK), during nitrogenase catalysis; (B, C) supplying electrons for nitrogenase assembly, coupling two [Fe_4S_4]-like clusters into a P-cluster on apo NifDK (B) or maturing a [Fe_8S_9] precursor on NifEN into an M-cluster via Mo/homocitrate insertion (C); and (D) serving as an active site for the binding and reduction of CO_2 and CO into hydrocarbons. The subunits of NifH are colored yellow and orange, the α- and β-subunits of NifDK are colored light green and light blue, and the α- and β-subunits of NifEN are colored green and blue. Atoms: Fe, orange; S, yellow; C, gray; Mo, teal; O, red; N, blue; P, tangerine; Mg, green; Al, light blue. PDB entries 1N2C,[10] 3U7Q[12] and 3PDI[23] are used to generate this figure.

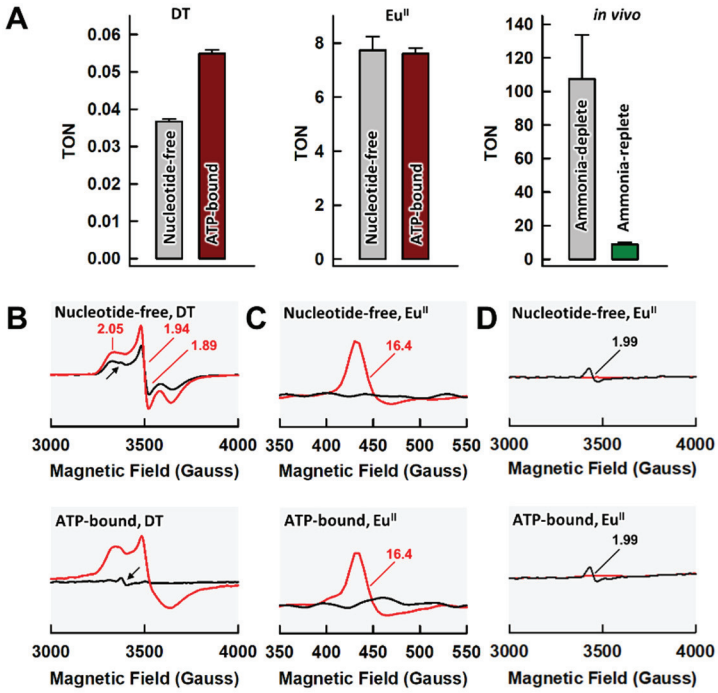

Figure 2. Reduction of CO_2 to CO by *Av*NifH. (A) Turnover numbers (TONs) of CO_2 reduction by *Av*NifH, either *in vitro* with dithionite (DT; left) or Eu^{II}-DTPA (Eu^{II}; middle) as a reductant, or *in vivo* upon depletion of ammonia in the growth media of an *Av*NifH-expressing strain (right). (B-D) Perpendicular (B, D)- and parallel (C)-mode EPR spectra of nucleotide-free (upper) and ATP-bound (lower) *Av*NifH in the presence (black) or absence (red) of CO_2. The *g* values are indicated. The arrows (B) indicate the $g \approx 2$ feature that appears in the DT-reduced samples in the presence of CO_2, which is more clearly visible in Eu^{II}-DTPA-reduced samples (D).

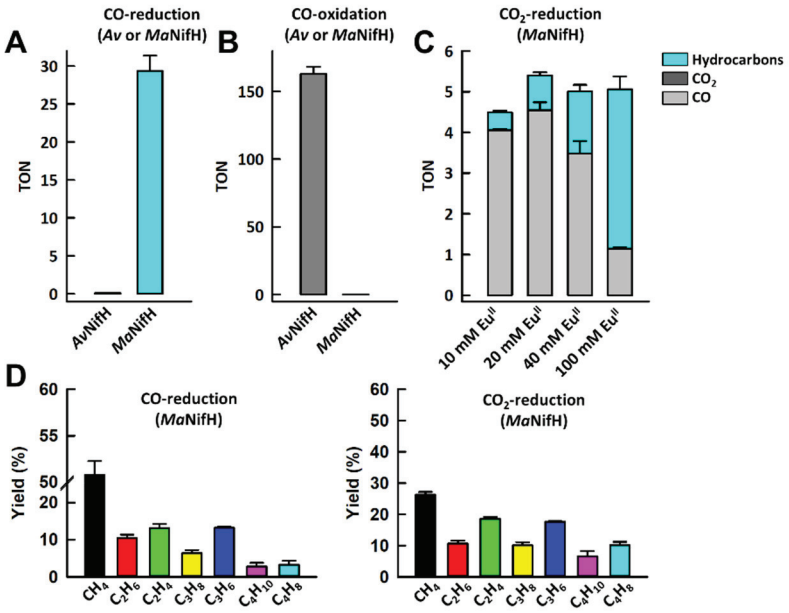

Figure 3. Differential reactivities of *Av*NifH and *Ma*NifH toward CO_2 and CO. (A, B) TONs of CO-reduction (A) or CO-oxidation (B) by *Av*NifH and *Ma*NifH. (C) TONs of CO_2-reduction by *Ma*NifH at increasing Eu^{II}-DTPA concentrations. (D) Product distributions of hydrocarbons generated from CO (left)- or CO_2 (right)-reduction by *Ma*NifH. TONs were calculated based on the total amounts of reduced C in products.

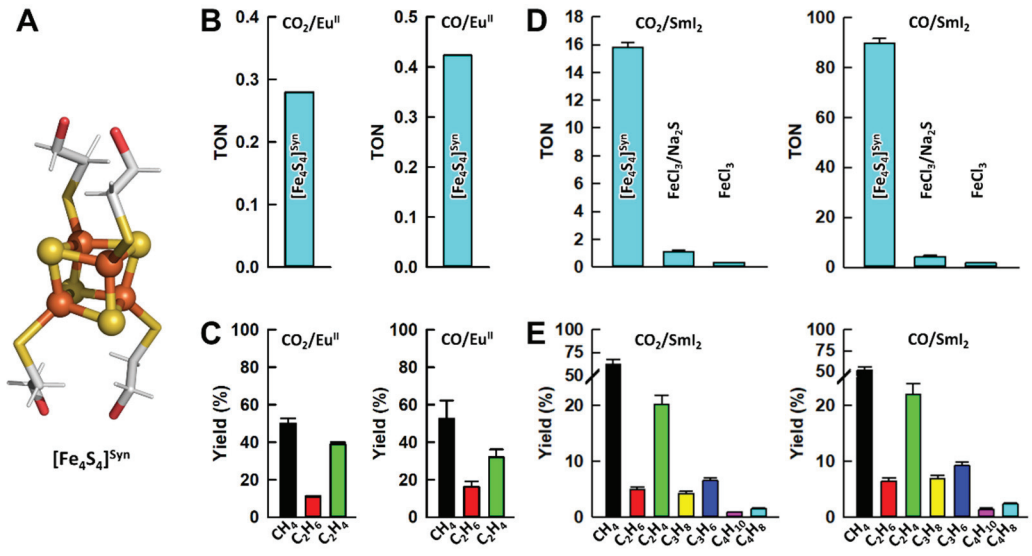

Figure 4. Reduction of CO_2 and CO by the $[Fe_4S_4]^{Syn}$ compound. (A) The structure of $[Fe_4S_4]^{Syn}$. (B, D) TONs and (C, E) hydrocarbon product distributions of CO_2- or CO-reduction by $[Fe_4S_4]^{Syn}$ in the presence of Eu^{II}-DTPA (B, C) or SmI_2 (D, E). TONs were calculated based on the total amounts of reduced C in products.

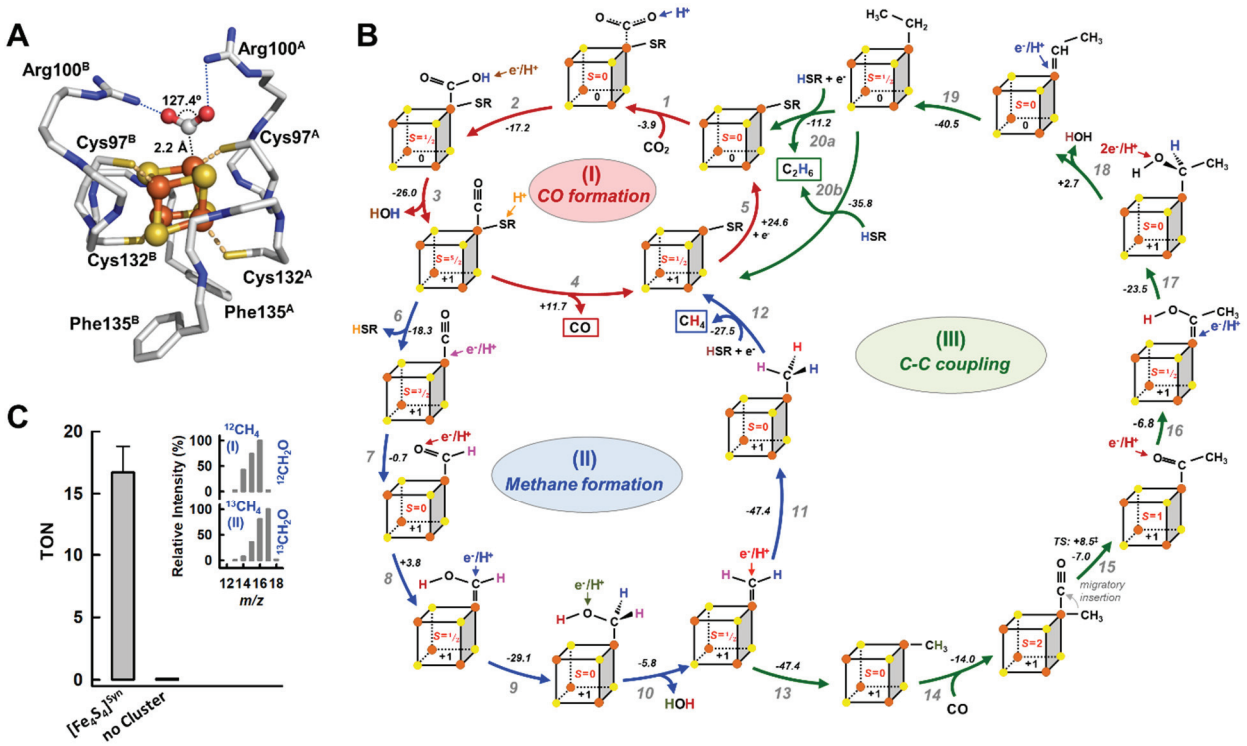

Figure 5. Mechanistic insights into CO_2 activation and reduction by $[Fe_4S_4]$ clusters. (A) DFT-predicted coordination of CO_2 to the $[Fe_4S_4]^0$ cluster (S=0) of *Av*NifH. Atoms: Fe, orange; S, yellow; C, grey; O, red. Residues from the two subunits of *Av*NifH are distinguished by superscripted A and B. (B) DFT-derived, energetically plausible reaction pathway of CO_2 reduction by $[Fe_4S_4]$ clusters. The calculated reaction energy (kcal mol^{-1}) is indicated for each step. (C) Reduction of CH_2O to CH_4 by $[Fe_4S_4]^{Syn}$. The fragmentation patterns of $^{12}CH_4$ and $^{13}CH_4$, generated from the reduction of $^{12}CH_2O$ and $^{13}CH_2O$, respectively, are shown in the inset.

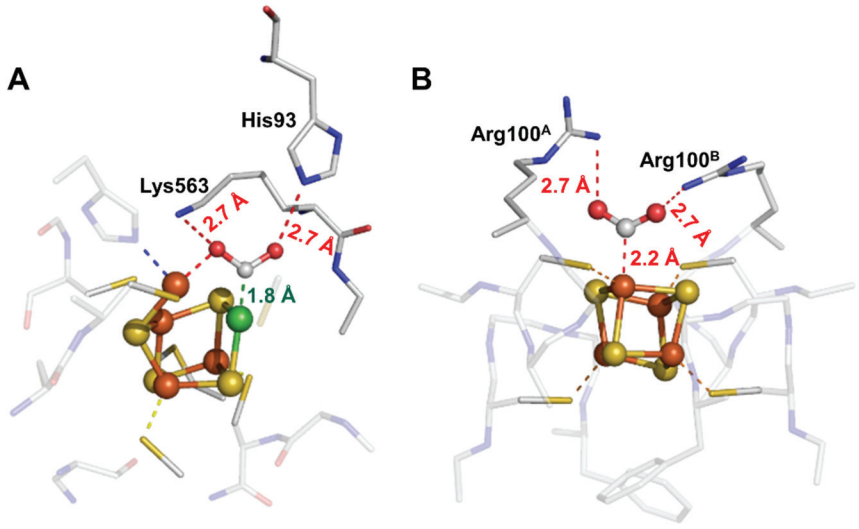

Figure 6. Comparison of CO_2 activation by Ni-CODH and *Av*NifH. (A) Activation of CO_2 by the C-cluster ([$NiFe_4S_4$]) of Ni-CODH involves coordination of C by Ni (a Lewis base) and O by a "dangling" Fe (a Lewis acid), and interaction of O with the side-chain groups of Lys and His via H-bonding. (B) Activation of CO_2 by the [Fe_4S_4] cluster of *Av*NifH involves coordination of C by Fe and interaction of O with the side-chain groups of a conserved Arg pair via H-bonding. Atoms: Ni, green; Fe, orange; S, yellow; C, grey; O, red.

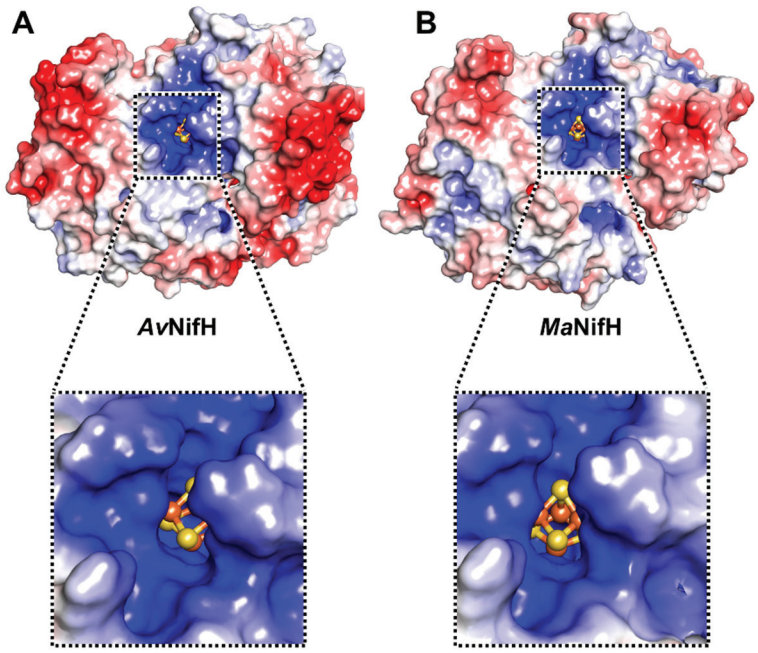

Figure 7. Comparison of the cluster accessibility in *Av*NifH and *Ma*NifH. Surface presentations of (A) the crystal structure of *Av*NifH and (B) the homology model of *Ma*NifH in the all-ferrous states reveal an improved surface accessibility of the [Fe_4S_4] cluster in *Ma*NifH that could further impact the reduction potential of the cluster. Atoms: Fe, orange; S, yellow. Negative and positive surface charges are colored red and blue, respectively.

Supplementary Information for

Reactivity of $[Fe_4S_4]$ Clusters toward C1 Substrates: Mechanism, Implications and Potential Applications

Chi Chung Lee, Martin T. Stiebritz and Yilin Hu

Department of Molecular Biology and Biochemistry, University of California, Irvine, California 92697-3900, United States

This PDF contains

Supplementary Figure S1

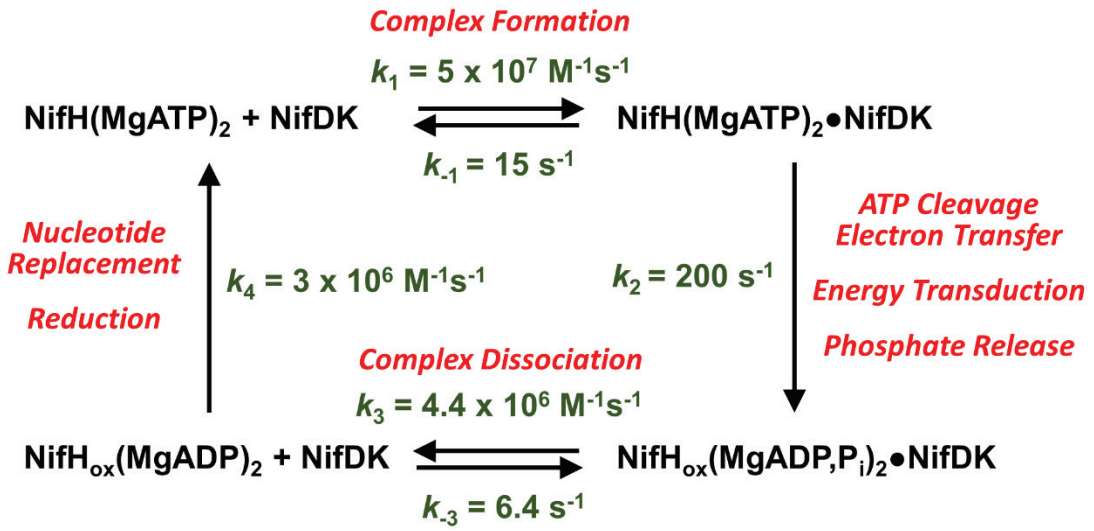

Figure S1. The "Fe protein cycle" of nitrogenase, which depicts the nucleotide-dependent association and dissociation between the Fe protein (NifH) and the MoFe protein (NifDK) during catalysis. Shown are the rate constants determined for the nitrogenase from *Klebsiella pneumonia*.[1]